Magnetic properties of ternary GICs[*]

M. Suzuki and I.S. Suzuki

Department of Physics,

State University of New York at Binghamton

(October 14, 2005)

1.   Classification of ternary GICs

1.1   Overview

Magnetic ternary GICs offer an opportunity to synthesize exotic compounds and to explore their novel physical properties. In these compounds two distinct guest species are intercalated into the graphite galleries between the host graphite layers. These two species may be present in the same gallery or may be isolated from one and other in different galleries. Magnetic ternary GICs not only enhance the versatility of magnetic binary GICs by adding another degree of freedom to the design of these compounds, but also offer wide possibilities for new route of their syntheses. Of our particular interest among the magnetic ternary GICs are the random mixture graphite intercalation compounds (RMGICs) and magnetic graphite intercalation compounds (GBICs).

1.2   Magnetic RMGICs

The magnetic RMGICs provide fascinating topics in magnetic phase transitions of 2D

---

random spin systems, including (i) spin glass phase and reentrant spin glass phase, (ii) cluster glass phase, (iii) random field effect, (iv) percolation behavior, and (v) an oblique phase arising from competing spin anisotropy between Ising and XY spin symmetry. The combination of spin frustration and randomness in RMGICs gives rise to a nonergodic many valley structure in free energy, leading to degenerate ground states. No single spin configuration is uniquely favored by all the interactions, suggesting that the magnetic ordered phase is intrinsically different from conventional forms of spin order. As far as we know, the magnetic properties of the following RMGICs have been reported so far: $Co_cMg_{1-c}Cl_2$ GICs (2D percolation system with a percolation threshold $c_p = 0.50$) (Nicholls, J.T., 1990b, Suzuki, I.S., 1993b, 1999a), $Co_cMn_{1-c}Cl_2$ GICs (Suzuki, I.S., 1991), $Ni_cMn_cCl_2$ GICs (Suzuki, I.S., 1992), and $Cu_cCo_{1-c}Cl_2$ GICs (Suzuki, I.S., 1994b, 1999b) (2D spin glass with competing ferromagnetic and antiferromagnetic interactions), and $Co_cNi_{1-c}Cl_2$ GICs (2D ferromagnetic random mixture with competing spin anisotropy) (Yeh, M. 1990, Suzuki, M., 1992). There are two methods for preparing RMGICs ($Co_cMg_{1-c}Cl_2$ GIC as an example): (i) intercalation of bulk random system $Co_cMg_{1-c}Cl_2$ into single crystals of kish graphite (SCKG) or HOPG in the presence of chlorine gas (740 Torr) (Suzuki, I.S., 1993b, 1999a), and (ii) intercalation of mixture of powdered $CoCl_2$ and $MgCl_2$ in the ratio of c: 1-c into SCKG and HOPG in a chlorine gas of three atmosphere (Nicholls, J.T., 1990b).

1.3   *Magnetic GBICs*

The magnetic GBICs offer possibilities for the formation of superlattices such as two different magnetic intercalate layers separated by a single graphite layer. A typical GBIC has a c-axis stacking sequence of $-G-I_1-G-I_2-G-I_1-G-I_2-G-...$, where two different intercalate layers (I_1 and I_2) alternate with a single graphite layer (G). This compound can be synthesized by a sequential intercalation. Stage-2 GICs are made with intercalant I_1, and the second intercalant I_2 is intercalated into the empty graphite galleries of stage-2

GICs. Because each layer is atomically flat with long range correlations in the c and a axis directions, and there is no interdiffusion between planes, GBICs form an ideal heterostructure. The magnetic properties of magnetic GBICs have attracted attention, partly because of the crossover behavior from two-dimensional (2D) to three-dimensional (3D).

As far as we know, the first GBIC was synthesized by Niess and Stump (Niess, R., 1978), who sequentially intercalated $TlBr_3$ and $TlCl_3$. In early 1980's several kinds of magnetic GBICs have been synthesized. Suzuki et al. (Suzuki, M., 1984b) have prepared a $CoCl_2$-$FeCl_3$ GBIC by a sequential intercalation of $FeCl_3$ into stage-2 $CoCl_2$ GIC. Hérold et al. (Hérold, A., 1985) have prepared several kinds of GBICs by a sequential intercalation of $AlCl_3$ and $GaCl_3$ into stage-2 $CoCl_2$ GIC and stage-2 $FeCl_3$ GIC, and by the sequential intercalation of $FeCl_3$ into a stage-2 $InCl_3$ GIC. The magnetic GBICs which have been synthesized since then are $NiCl_2$-$FeCl_3$ GBIC, $FeCl_3$-YCl_3 GBIC, $MnCl_2$-$AlCl_3$ GBIC, $CrCl_3$-$MnCl_2$ GBIC, $CrCl_3$-$CdCl_2$ GBIC, and $CrCl_3$-$AlCl_3$ GBIC, $Co_cNi_{1-c}Cl_2$-$FeCl_3$ GBIC, $Co_cMn_{1-c}Cl_2$-$FeCl_3$ GBIC, and $Cu_cCo_{1-c}Cl_2$-$FeCl_3$ GBIC. Among them, there have been several studies on the magnetic properties of magnetic GBICs: $CoCl_2$-$FeCl_3$ GBIC (Suzuki, M., 1984b, Hérold, A., 1985), $CoCl_2$-$GaCl_3$ GBIC (Rosenman, I., 1986), $NiCl_2$-$FeCl_3$ GBIC (Rancourt, D.G. 1988), $CrCl_3$-$NiCl_2$ GBIC (Rancourt, D.G., 1990), $CrCl_3$-$CoCl_2$ GBIC (Flandrois, S., 1994), $CrCl_3$-$CdCl_2$ GBIC (Chehab, S., 1991, 1992), $CrCl_3$-$MnCl_2$ GBIC (Chehab, S., 1991, 1992), $Co_cNi_{1-c}Cl_2$-$FeCl_3$ GBICs (Suzuki, I.S., 1994a), $Co_cMn_{1-c}Cl_2$-$FeCl_3$ GBICs (Suzuki, I.S., 1995), and $Cu_cCo_{1-c}Cl_2$-$FeCl_3$ GBICs (Suzuki, I.S., 1997, 2000).

2.   Stage-2 $Co_cMg_{1-c}Cl_2$ GICs: Percolation systems

2.1   Overview

When one of the intercalants is magnetic and the other is nonmagnetic, RMGIC provides a model system for studying two-dimensional (2D) site-diluted random spin

systems. The interplanar exchange interactions between magnetic ions in different intercalate layers is much weaker than the intraplanar exchange interactions between magnetic ions in the same intercalate layer. Stage-2 $Co_cMg_{1-c}Cl_2$ GICs are typical examples of 2D XY-like site-diluted random spin systems. In these compounds a part of Co^{2+} ions on the triangular lattice sites is replaced by nonmagnetic Mg^{2+} ions. It is theoretically predicted that the percolation threshold c_p is equal to 0.5 for the 2D triangular lattice with nearest neighbor (N.N.) intraplanar exchange interaction. For $c<c_p$ there is no long range spin order at any temperature T. The point ($T = 0$ and $c = c_p$) in the T-c plane is the multi-critical point where the thermally driven critical behavior ($c = c_p$ and $T \rightarrow 0$) and the geometrically driven critical behavior ($c \rightarrow c_p$ and $T = 0$) merge.

There have been several publications on the magnetic phase transitions of stage-1 $Co_cMg_{1-c}Cl_2$ GICs and stage-2 $Co_cMg_{1-c}Cl_2$ GICs. Nicholls and Dresselhaus (Nicholls, J.T., 1990b) have studied the effect of dilution with nonmagnetic ions on the magnetic phase transition in stage-1 $Co_cMg_{1-c}Cl_2$ GICs. They have shown that the critical temperature T_c is extrapolated to zero at the critical concentration $c = 0.65$, which is larger than $c_p = 0.5$. They have claimed that such a deviation of the critical concentration ($c = 0.65$) from $c_p = 0.5$ is due to a possible 15% random distribution of voids inside the intercalate layers. Suzuki et al. (Suzuki, I.S., 1993b, 1994b) have studied the magnetic phase transitions of stage-2 $Co_cMg_{1-c}Cl_2$ GICs. They have measured the temperature dependence of the dispersion χ'_{aa} only at $f = 330$ Hz: it exhibits a single peak at a temperature T_p. In spite of the fact that χ''_{aa} shows two peaks at critical temperatures T_{cu} and T_{cl}, the peak temperature T_p was identified as a critical temperature ($T_{cl}<T_p<T_{cu}$). They have found that the reduced critical temperature of stage-2 $Co_cMg_{1-c}Cl_2$ GIC is almost the same as that of pristine $Co_cMg_{1-c}Cl_2$ for $c>0.7$. The effect of the dimensionality on the dilution with Mg^{2+} ions becomes significant below $c \approx 0.7$. The percolation threshold for stage-2 $Co_cMg_{1-c}Cl_2$ GICs is close to that predicted for the 2D triangular lattice with N.N. exchange interaction ($c_p = 0.5$). Suzuki and Suzuki (Suzuki,

I.S., 1999a) have studied the percolation and spin glass behavior of these compounds with $0.3 \le c \le 1$ using SQUID AC magnetic susceptibility (χ'_{aa} and χ''_{aa}) and SQUID DC magnetization. The critical temperature T_{cl} decreases to zero at the percolation threshold $c_p = 0.5$, while T_{cu} above c_p decreases with decreasing Co concentration and may be connected to a crossover temperature T_X below c_p. A spin glass-like behavior is observed for $c = 0.3$ and 0.46.

2.2   Scaling concept in percolation behavior

Here we present a simple review on the phase transition of diluted ferromagnet with nearest-neighbor interactions on the regular lattice (Birgeneau, R.J., 1984, Stinchcombe, R.B., 1983). For simplicity we assume that the pure system ($c = 1$) undergoes an ordinary phase transition at $T_c(c = 1)$. A part of the magnetic ions may be readily replaced by nonmagnetic ions. With increasing dilution the critical temperature $T_c(c)$ decreases rapidly at $c = c_p$ (= 0.5), where c_p is the site percolation concentration for the N.N. triangular lattice problem (Essam, J.W., 1972). For $c < c_p$ no phase transition can exist since the system breaks up into isolated finite clusters that cannot sustain long-range order. The mean size of the isolated finite clusters diverges as c approaches c_p. For c just above c_p in addition to the finite clusters analogous to the finite clusters below c_p, there appears an infinite percolation cluster which provides linkage paths. The structure of this infinite percolation cluster becomes increasingly more ramified as c approaches c_p ($c > c_p$). Consequently, the 1D characteristics will become more and more pronounced. The existence of these 1D characteristics suggest that the thermal properties is similar to those of a 1D system. From this idea, a scaling theory has been developed for the percolation region which results in a correlation length $\xi(c, T)$ given by

$$1/\xi(c,T) = |c - c_p|^{v_p} F(\xi_{1d} |c - c_p|^{\phi}), \qquad (1)$$

where ξ_{1d} is the correlation length of the 1D system at T. The system undergoes a lattice connectivity-driven percolation transition on approaching along the path $T = 0$ and $c \to c_p$, where the correlation length and the susceptibility are described by $\xi(c,0) \approx \xi_p \approx |c - c_p|^{-\nu_p}$, and $\mathcal{X}(c,0) \approx |c - c_p|^{-\gamma_p}$, respectively. The system also undergoes a thermal driven phase transition with critical exponents $\nu_T = \nu_p/\phi$ and $\gamma_T = \gamma_p/\phi$ on approaching along $c = c_p$ and $T \to 0$. The exponent ϕ is a cross-over exponent ($\phi = \nu_p/\nu_T = \gamma_p/\gamma_T$) and $\phi = 1$ for the 2D Ising model and $\phi = 1.43$ for the Heisenberg model. The function F(x) is a scaling function of x: $F(x) \approx x^{-\nu_T}$ in the limit $x \to 0$ ($c = c_p$), and constant in the limit $x \to \infty$ ($T = 0$). Correspondingly the correlation length ξ can be expressed by $\xi = \xi_T \approx (\xi_{1d})^{\nu_T}$, and $\xi = \xi_p$, respectively. The thermal correlation length is determined by the 1D correlation length ξ_{1d}.

In the region $c<c_p$, the growth of the correlation length is limited by the size of the percolation cluster ξ_p. For the 1D XY system the correlation length ξ_{1d} is proportional to $1/T$: more exactly we have $\xi_{1d} = 2/t$, where $t = k_B T/[2|J|S(S + 1)]$ and J is the intrachain exchange constant. Therefore, the crossover line $T_x(c)$ is described by $T_x(c) \approx |c - c_p|^{\phi}$ for $\xi_T \approx \xi_p$. For $T<T_x(c)$, one has $\xi_T>\xi_p$, which implies that all the spins belonging to a characteristic cluster are essentially ferromagnetically ordered. For $T>T_x(c)$, one has $\xi_p > \xi_T$, implying that the fractal structure of the percolation cluster dominates the thermodynamic behavior of the system.

The critical temperature $T_c(c)$ for $c>c_p$ can also be extracted from this scaling form. The correlation length diverges when F(x) becomes infinite at some point x_0: $x_0 = \xi_{1d} |c - c_p|^{-\phi}$. Since ξ_{1d} is proportional to $1/T$ for 1D XY systems, the critical temperature $T_c(c)$ is determined as $T_c(c) \approx |c - c_p|^{\phi}$, implying that $T_c(c)$ for $c>c_p$ has the same c-dependence as $T_x(c)$ for $c<c_p$.
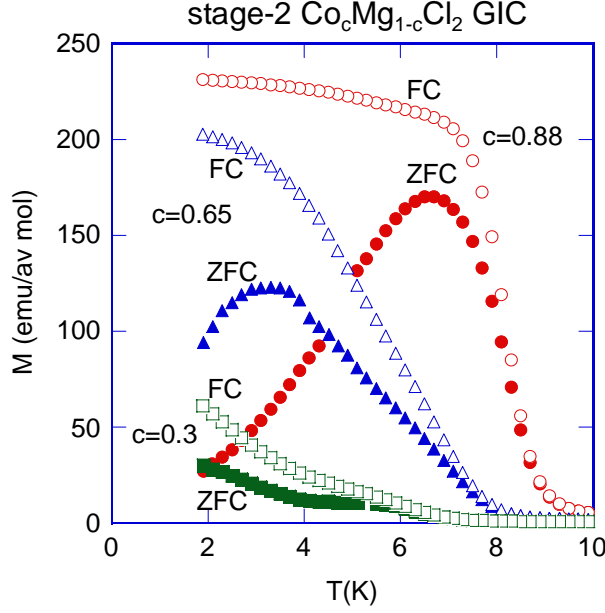
2.3   SQUID DC magnetization

Figure 1. T dependence of M_{FC} and M_{ZFC}. $H \perp$ c and. $H = 1$ Oe. $c = 0.88$ ($\bigcirc$, $\bullet$), 0.65 ($\triangle$, $\blacktriangle$) and 0.3 ($\square$, $\blacksquare$). (Suzuki, I.S., 1999a)

Figure 1 shows the temperature dependence of zero-field magnetization M_{ZFC} and field-cooled magnetization M_{FC} for stage-2 $Co_cMg_{1-c}Cl_2$ GICs with $c = 0.88$, 0.65, and 0.3 in the presence of an external field H (= 1 Oe) along the c plane (Suzuki, I.S., 1999a). For $c = 1$ M_{ZFC} exhibits a broad peak at $T_p^{ZFC} = 8.2$ K between T_{cl} and T_{cu}, with increasing temperature. The deviation of M_{FC} from M_{ZFC} occurs below a characteristic temperature $T_f = 10.7$ K. It drastically increases with further decreasing T. The temperature dependence of M_{ZFC} and M_{FC} for $c = 0.88$ is similar to that for $c = 1$, where $T_p^{ZFC} = 6.6$ K and $T_f = 9.7$ K. For $c = 0.65$ M_{ZFC} has a broad peak at $T_p^{ZFC} = 3.3$ K. It gradually decreases with increasing temperature and reduces to zero around $T_f = 8.7$ K. The magnetization M_{FC} deviates from M_{ZFC} below T_f and gradually increases with decreasing temperature. The temperature dependence of M_{ZFC} and M_{FC} for $c = 0.61$ and 0.46 is similar to that for $c = 0.65$, where $T_p^{ZFC} = 2.5$ K and $T_f = 7.8$ K for $c = 0.61$, and $T_p^{ZFC} = 3.6$ K and $T_f = 8.5$ K for $c = 0.46$. We note that the values of T_p^{ZFC} and T_f for $c = 0.46$ are larger than those for $c = 0.61$, respectively. As shown in Fig.1, the temperature dependence of M_{ZFC} for $c = 0.3$ is different from that for $c \geq 0.46$. The decrease of M_{ZFC} with increasing temperature occurs in two steps. It decreases with decreasing temperature

below 4K. It becomes constant between 4.1 and 5.7 K, and decreases with further increasing temperature. The magnetization M_{FC} deviates from M_{ZFC} below T_f (= 7.9 K) and increases with decreasing T.

2.4   SQUID AC magnetic susceptibility

Figures 2 (a) - (d) show the temperature dependence of the absorption χ''_{aa} at various
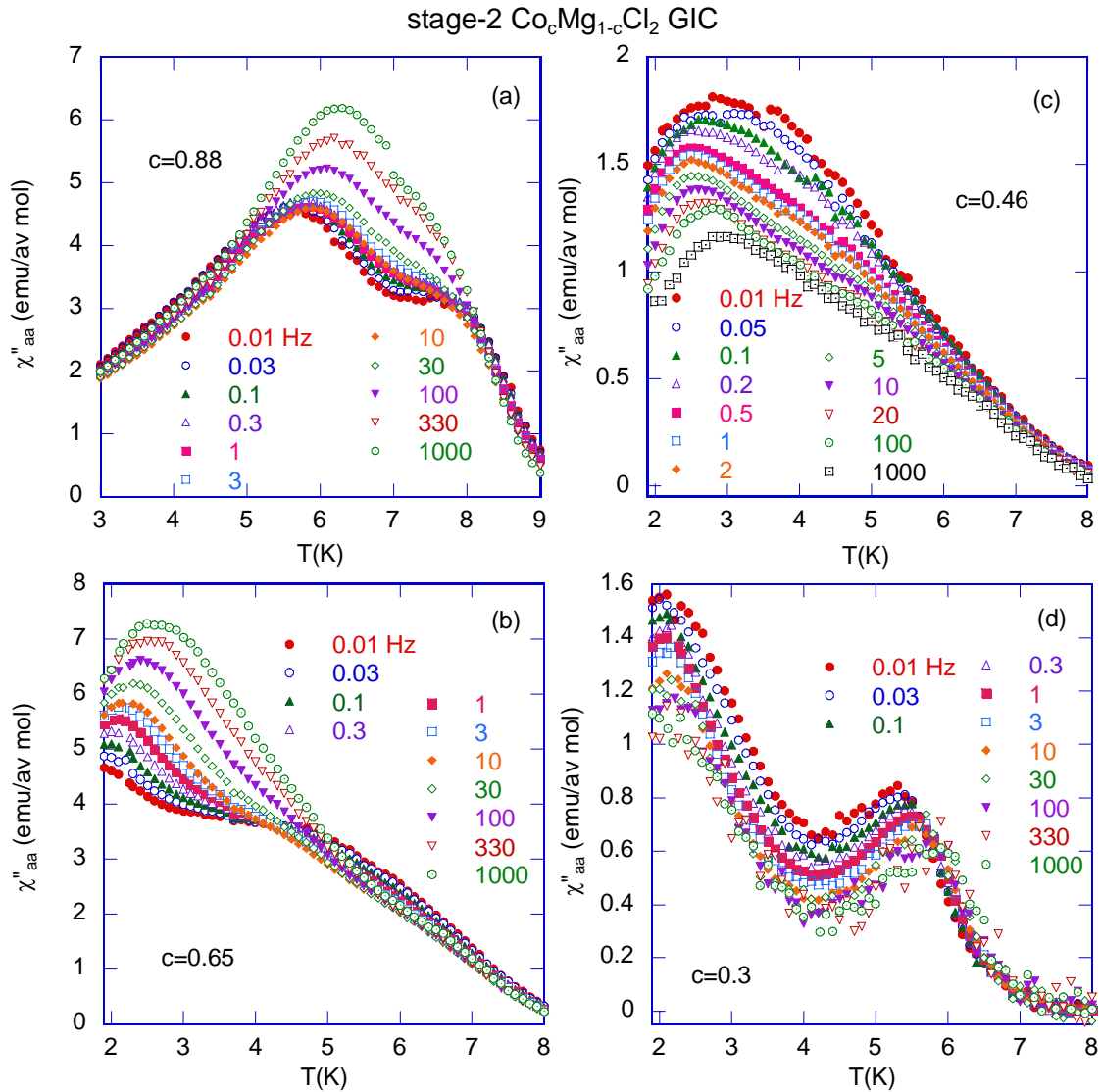

Figure 2. T dependence of χ''_{aa} at various frequencies for stage-2 $Co_cMg_{1-c}Cl_2$ GICs. H = 0 and $h \perp c$. h = 50 mOe. $0.01 \leq f \leq 1000$ Hz. (a) c = 0.88, (b) 0.65, (c) 0.46, and (d) 0.3. (Suzuki, I.S., 1999a)

frequency for stage-2 $Co_cMg_{1-c}Cl_2$ GICs with $c = 0.88$, 0.65, 0.46, and 0.3 in the absence of magnetic field (Suziki, I.S., 1999a). For $c = 1$ the absorption χ''_{aa} shows two peaks at T_{cu} and T_{cl}, and a small peak around 8.4 K coinciding with the peak temperature of χ'_{aa}. The value of T_{cu} (= 8.9 - 9.0 K) is almost independent of frequency, while the value of T_{cl} slightly increases with increasing frequency (T_{cl} = 6.78 K for f = 0.01 Hz and 7.20 K for f = 1 kHz), showing evidence for a cluster glass phase below T_{cl}.

In Fig.2(a) χ''_{aa} for $c = 0.88$ exhibits a broad peak at T_{cl} which shifts to the high temperature side with increasing f: T_{cl} = 5.61 K at f = 0.01 Hz and 6.27 K at f = 1 kHz. It also has a shoulder at T_{cu} which slightly decreases with increasing f: T_{cu} = 7.97 K at f = 0.01 Hz and 7.71 K at f = 1 kHz. The absorption χ''_{aa} for $c = 0.74$ exhibits a very broad peak at T_{cu} which shifts to the high temperature side with increasing frequency: T_{cu} = 4.17 K at f = 0.1 Hz and 4.59 K at f = 1 kHz.

In Fig.2(b) χ''_{aa} for $c = 0.65$ has a broad peak at T_{cl} and a shoulder at T_{cu} observable only for $f \geq 0.1$ Hz and $0.01 \leq f \leq 1$Hz, respectively. The critical temperature T_{cl} increases with increasing frequency (1.95 K for f = 0.1 Hz and 2.61 K for f = 1 kHz), while T_{cu} is almost independent of frequency: T_{cu} = 4.52 - 4.61 K. For $c = 0.61$ χ''_{aa} has a broad peak at T_{cl} and a shoulder at T_{cu} observable only for $f \geq 1$ Hz and $0.01 \leq f \leq 20$ Hz, respectively. The critical temperature T_{cl} increases with increasing frequency (1.96 K for f = 1 Hz and 2.45 K for f = 1 kHz), while T_{cu} is almost independent of frequency: T_{cu} = 4.48 - 4.64 K.

In Fig.2(c) χ''_{aa} for $c = 0.46$ has a very broad peak for $2.5 \leq T \leq 3$ K. Note that this peak temperature exhibits a complicated frequency dependence. It decreases from 2.8 K at f = 0.01 Hz with increasing frequency and becomes constant (= 2.5 K) between 0.2 and 5 Hz. It increases in turn with further increasing frequency and reaches 3.0 K at f = 1 kHz, suggesting spin glass-like behavior for $10 \leq f \leq 1000$ Hz. In Fig.2(d) χ''_{aa} for $c = 0.3$ has two peaks around 2.0 - 2.24 K and T_{SG} (= 5.28 - 5.84 K). The peak at T_{SG} shifts to the high temperature side with increasing frequency, suggesting the existence of spin glass behavior.

2.5 *Magnetic phase diagram*

Figure 3 shows the critical temperatures as a function of Co concentration. For convenience the critical temperatures T_{cu} and T_{cl} (denoted by solid circles and solid triangles, respectively) for $c>0.65$ are defined as a temperature where χ''_{aa} at $f = 0.01$ Hz for $c = 0.3, 0.46, 0.88$, and 1, χ''_{aa} at $f = 0.1$ Hz for $c = 0.65$ and 0.74, and χ''_{aa} at $f = 1$ Hz for $c = 0.61$ exhibit either a cusp or a shoulder. Note that the values of T_{cu} and T_{cl} are weakly dependent on frequency. For $c<0.5$ χ''_{aa} at $f = 0.01$ Hz still has a broad peak at a characteristic temperature (denoted by solid square in Fig.3), which should be distinguished from T_{cu} and T_{cl}. This temperature is not a true critical temperature because there is no long range spin order. In Fig.3 we also show the peak temperatures of χ'_{aa} at $f = 0.1$ Hz and M_{ZFC} as a function of c. For $0.61 \leq c \leq 1$ the peak temperatures of χ'_{aa} and M_{ZFC} are almost the same and between T_{cu} and T_{cl}. For $c = 0.46$ and 0.3 the peak temperatures of χ'_{aa} are almost the same as those of χ''_{aa}.

The features of Fig.3 are summarized as follows. The critical temperature T_{cl} decreases with decreasing Co concentration c for $0.61 \leq c \leq 1$. The critical temperature T_{cl}
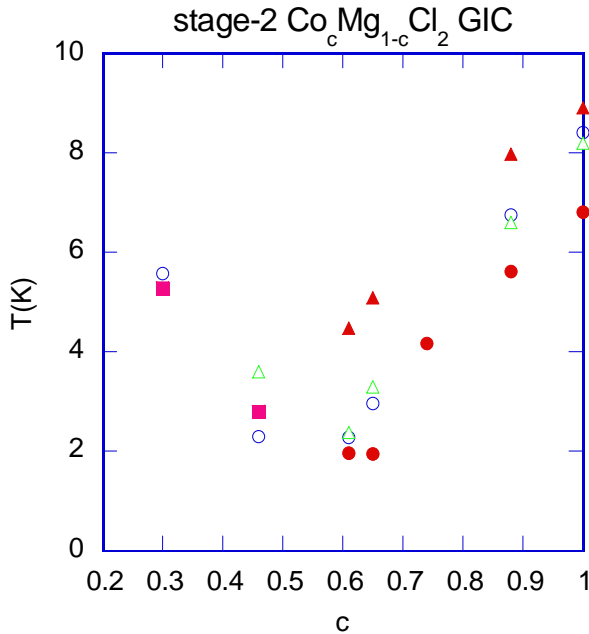

Figure 3. Magnetic phase diagram of stage-2 $Co_cMg_{1-c}Cl_2$ GICs. The critical temperatures [T_{cu} (▲) and T_{cl} (●)] are defined as a temperature where χ''_{aa} at $f = 0.01$ Hz for $c = 0.88$, and 1, χ''_{aa} at $f = 0.1$ Hz for $c = 0.65$ and 0.74, and χ''_{aa} at $f = 1$ Hz for $c = 0.61$ exhibit either a cusp or a shoulder. The peak temperatures of χ''_{aa} at $f = 0.01$ Hz for $c = 0.46$ and 0.3 are denoted by solid square (■). The peak temperatures of χ'_{aa} (○) and M_{ZFC} (Δ) for each concentration are also shown. (Suzuki, I.S., 1999a)

tends to reduce to zero around $c = 0.5$, corresponding to the percolation threshold for the 2D random spins on the triangular lattice. The temperature T_{cu} also decreases with decreasing Co concentration for $0.65 \leq c \leq 1$. One cannot conclude from Fig.3 that T_{cu} may tend to reduce to zero around $c = 0.5$. However, one may say that T_{cu} for $0.65 \leq c \leq 1$ is connected to the crossover temperature $T_X(c)$ for $0.3 \leq c \leq 0.46$, where $\xi_T = \xi_p$. The peak temperature of M_{ZFC} decreases with decreasing Co concentration c, showing a local minimum around $c = 0.5$. It increases in turn with further decreasing Co concentration, suggesting the existence of $T_X(c)$.

The magnetic phase transition of stage-2 $Co_cMg_{1-c}Cl_2$ GICs with $0.65 \leq c \leq 0.88$ is similar to that of stage-2 $CoCl_2$ GIC (Suzuki, M., 1998a). Between T_{cl} and T_{cu} the 2D ferromagnetic long rang order is established. The in-plane spin correlation length grows to the order of the island size at T_{cl}. Below T_{cl} a 3D antiferromagnetic long range order develops through effective interplanar interactions including interisland interactions between islands in adjacent intercalate layers. The critical temperature T_{cl} for $c = 1$, 0.88, and 0.65 slightly increases with increasing frequency, suggesting that the 3D antiferromagnetic phase has partly a characteristic of cluster glass phase, where each island plays the role of each spin in spin glass behavior. The spin directions of ferromagnetic islands are frozen because of frustrated inter-island interactions.

2.6 Spin glass behavior below c_p

We discuss the frequency dependence of the peak temperature in $\chi_{aa}''(\omega)$ for $c = 0.3$ and 0.46 below c_p. The peak temperature T_{SG} for $c = 0.3$ increases with increasing frequency. In contrast, the frequency dependence of the peak temperature in $\chi_{aa}''(\omega)$ for $c = 0.46$ is rather different from that for $c = 0.3$. The peak temperature decreases from 2.8 K to 2.5 K with increasing frequency for $0.01 \leq f \leq 0.2$ Hz. It becomes constant for $0.2 \leq f \leq 5$ Hz, and in turn increases with further increasing frequency for $0.5 \leq f \leq 1000$ Hz.
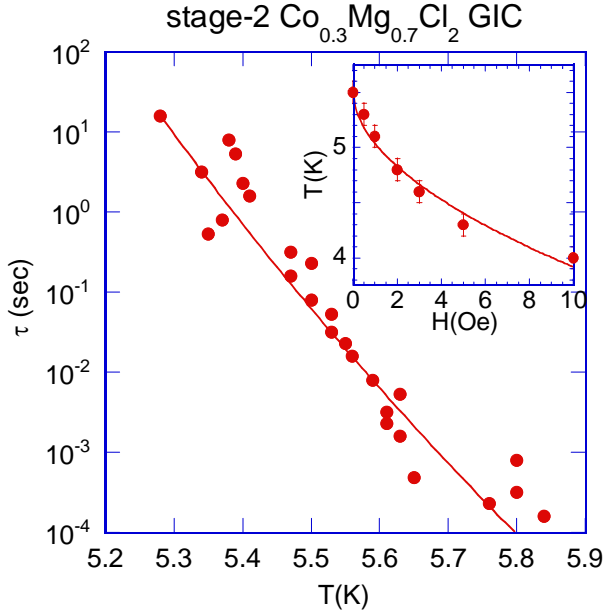
stage-2 Co$_{0.3}$Mg$_{0.7}$Cl$_2$ GIC

Figure 4. Relaxation time τ vs T for stage-2 Co$_c$Mg$_{1-c}$Cl$_2$ GIC with $c = 0.3$. The solid line does not denote a least squares fit of the data to eqn (2). The H dependence of peak temperature in χ_{aa}'' ($c = 0.3$) at $f = 1$ Hz is shown in the inset where the solid line denotes a least squares fit of the data to the power law form. (Suzuki, I.S., 1999a)

How can we explain the increase of the peak temperature with increasing f? There may be two possibilities: (i) superpamagnet and (ii) spin glass phase. The superparamagnet is formed of finite clusters of spins which do not interact with each other (Mydosh, J.A., 1993). When the relevant anisotropy is uniaxial, there are two equivalent states of opposite magnetization for each cluster. At finite temperatures thermal fluctuations give some probability of overcoming the energy barrier E$_a$. The relaxation time between two states of equal energy is given by thermal activation (Arrehenius law) $\tau = \tau_0 \exp(E_a/k_B T)$, where τ_0 is a microscopic limiting relaxation time usually $\approx 10^{-9}$ sec. The least squares fit of the data (the peak temperature vs f) for $c = 0.3$ to an Arrhenius law described by $f = f_0 \exp(-T_a/T)$ yields the completely unphysical values of f_0 (= 5.57 x 10^{58}) and T_a (= 741 K). Therefore the frequency dependence of the peak temperature cannot be described by an Arrhenius law.

Next we consider the possibility of spin glass behavior for $c = 0.3$. Figure 4 shows the average relaxation time τ for $c = 0.3$ as a function of temperature, where τ is determined using the relation that the peak of χ_{aa}'' vs T appears when $\omega\tau = 1$ is satisfied. The average relaxation time τ divergingly increases with decreasing temperature. The most likely

source for such a dramatic divergence of τ is a critical slowing down. The relaxation time

τ can be described by a power law form

$$\tau = \tau_0 (T/T^* - 1)^{-x},\qquad(2)$$

where x is a critical exponent and T^* is a finite critical temperature. No attempt on the least squares fit of the data for $5.28 \leq T \leq 5.82$ K to eqn (2) has been successful so far. We note that the solid line in Fig.4 is described by eqn (2) with $T^* = 3.86$ K and $y = 38.6$. The value of y is unphysical.

In the inset of Fig.4 we show the field dependence of $T_{SG}(H)$ for c = 0.3. The peak temperature $T_{SG}(H)$ is related to magnitude of H through a power law form described by

$$T_{SG}(H) = T_{SG}(H = 0)\left[1 - \left(\frac{H}{H_0}\right)^{1/a}\right],\qquad(3)$$

where a is an exponent. The least squares fit of the data of T_{SG} vs H in the field range $0 \leq H \leq 10$ Oe yields a = 1.88 ± 0.17 and $H_0 = 104 \pm 5$ Oe, where $T_{SG}(H = 0) = 5.5$ K. The exponent a is a little larger than that predicted by Almeida and Thouless (Almeida, J.R.L., 1978) for the H dependence of freezing temperature at the transition between the paramagnetic phase and spin glass phase. These two observations suggest the occurrence of spin-glass like behavior for c = 0.3. The competition between ferromagnetic intraplanar interactions and effective antiferromagnetic interplanar exchange interactions, which may be too weak to cause a 3D antiferromagnetic phase, gives rise to a spin frustration effect.

2.7   *Crossover temperature*

We discuss how the existence of small islands in the intercalate layers affects the percolation behavior. The intercalate layers of stage-2 $Co_cMg_{1-c}Cl_2$ GIC are formed of small islands with size L. The magnetic behavior of this system is expected to be strongly dependent on the magnitudes of ξ_p and L which are independent of temperature. The size L depends on the amount of charge transfer from graphite layers to intercalate layers during intercalation, while ξ_p is a geometrical size depending only on c. Here we consider the following two cases: (i) $c \approx c_p$ and $c > c_p$ and (ii) $c \approx c_p$ and $c < c_p$ where $\xi_p > L$. In case (i), a 2D ferromagnetic long range spin order may exist inside infinite clusters. The spin ordering process is essentially the same as that in pure stage-2 $CoCl_2$ GIC. When the in-plane spin correlation length ξ is on the same order as L, the interisland interactions becomes significant as well as the intraisland interactions. Although the growth of ξ is partly limited by the existence of small islands, ξ continues to grow and becomes larger than L. The 2D ferromagnetic spin order is established below T_{cu} where $\xi \gg L$. The 3D antiferromagnetic spin order occurs below T_{cl} where the effective antiferromagnetic interplanar exchange interaction given by $J'_{eff} = J'S^2(\xi/a)^2$. becomes comparable to J.

In case (ii), there are only isolated finite clusters having the size ξ_p, which is larger than L. When ξ is comparable to L, the interisland interactions becomes significant as well as the intraisland interactions. Since the growth of ξ is limited by ξ_p in the finite clusters, no true 2D ferromagnetic long range spin order occurs. For $\xi \approx \xi_p$ the effective antiferromagnetic interplanar interaction J'_{eff} [$\approx J'S^2(\xi_p/a)^2$] may be relatively weaker than J. Nevertheless the competition between these interactions may lead to a short-range spin-glass behavior below T_{SG}. The temperature T_{SG} may correspond to the crossover temperature $T_x(c) \approx |c-c_p|^\phi$ which is obtained from the condition that $\xi_T \approx \xi_p$. Note that the Co concentration dependence of T_x is similar to that of T_{cu} for $c > c_p$.

3.   Stage-2 $Cu_cCo_{1-c}Cl_2$ GICs

3.1 *Magnetic phase diagram*

Stage-2 $Cu_cCo_{1-c}Cl_2$ GICs magnetically behave like a 2D XY random spin system with competing ferromagnetic and antiferromagnetic short-ranged exchange interactions. In each intercalate layer Cu^{2+} and Co^{2+} spins are randomly distributed on the triangular lattice, forming 2D random spin systems. The interaction between Co^{2+} spins is ferromagnetic, while the interaction between Cu^{2+} spins is antiferromagnetic: $J(Co\text{-}Co) =$ 7.75 K and $J(Cu\text{-}Cu) = $ -33.63 K (Suzuki, M., 1994b). The interaction between Cu^{2+} and Co^{2+} spins is ferromagnetic. The sign of Θ changes around $c = 0.8$, indicating that the competition between intraplanar ferromagnetic and antiferromagnetic exchange interactions occurs.

Figure 5 shows the magnetic phase diagram of stage-2 $Cu_cCo_{1-c}Cl_2$ GICs which is determined from SQUID AC magnetic susceptibility (Suzuki, I.S., 1998b, 1999b, Suzuki, M., 2000). For $0 \leq c \leq 0.3$ the system undergoes two phase transitions at T_{cu} and T_{cl} ($T_{cu} > T_{cl}$). Below T_{cu} a 2D ferromagnetic order is established in each intercalate layer. Below T_{cl} there appears a 3D antiferromagnetic phase with the 2D ferromagnetic layers being antiferromagnetically coupled along the c axis. For $0.4 \leq c \leq 0.9$ the system undergoes a phase transition at T_{cl} and a reentrant spin glass (RSG) transition at T_{RSG} ($< T_{cl}$). The value of T_{RSG} is almost independent of Cu concentration. For $0.9 < c \leq 0.93$ the
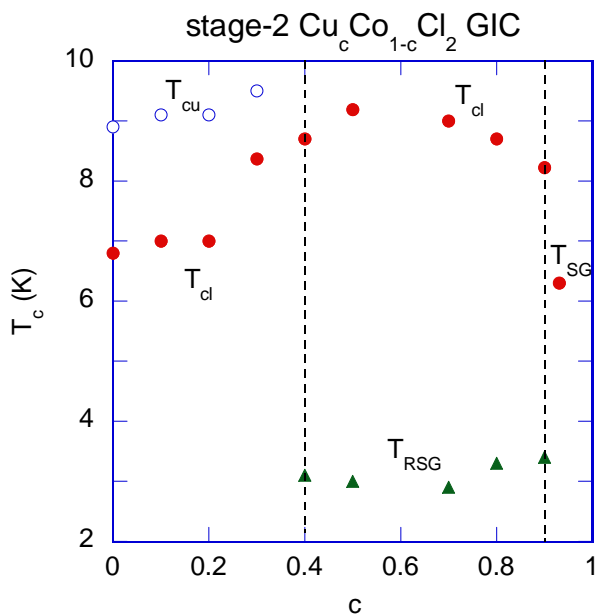

Figure 5. Magnetic phase diagram of stage-2 $Cu_cCo_{1-c}Cl_2$ GICs, where peak temperatures of χ''_{aa} at f = 0.1 Hz are plotted for each Cu concentration. (Suzuki, I.S., 1999b)

15

system undergoes a spin glass (SG) transition at T_{SG}. For $c \approx 1$ no phase transition is observed at least above 0.3 K, partly because of the frustrated nature of the 2D antiferromagnet on the triangular lattice. The value of T_{cl} increases with increasing Cu concentration and reaches a maximum around $c = 0.5$, where the probability $P(Cu\text{-}Co)$ of finding Cu-Co bonds becomes a maximum. Such an enhancement of T_{cl} suggests that ferromagnetic interaction $J(Cu\text{-}Co)$, which is comparable to or larger than $J(Co\text{-}Co)$ above $c = 0.5$, plays an important role for the ferromagnetic long range order in each intercalate layer.

3.2   Reentrant spin glass phase

Figure 6 shows the temperature dependence of $\chi_{aa}^{"}$ for c = 0.8 at various frequency (Suzuki, I.S., 1999b). The absorption $\chi_{aa}^{"}$ has two peaks at T_{RSG} (= 3 - 6 K) and T_{cl} (= 9.20 - 9.30 K). The peak at T_{RSG} shifts to the high temperature side with increasing frequency. The magnetization M_{ZFC} has a shoulder around 3.5 K and a peak at $T_0 = 9.0$ K. The deviation of M_{ZFC} from M_{FC} appears below $T_f = 12.5$ K, implying the irreversible effect of magnetization occurring below this temperature. The magnetization M_{FC} drastically increases with decreasing temperature below ≈ 10 K, suggesting that the 2D ferromagnetic order is established in the intercalate layers.
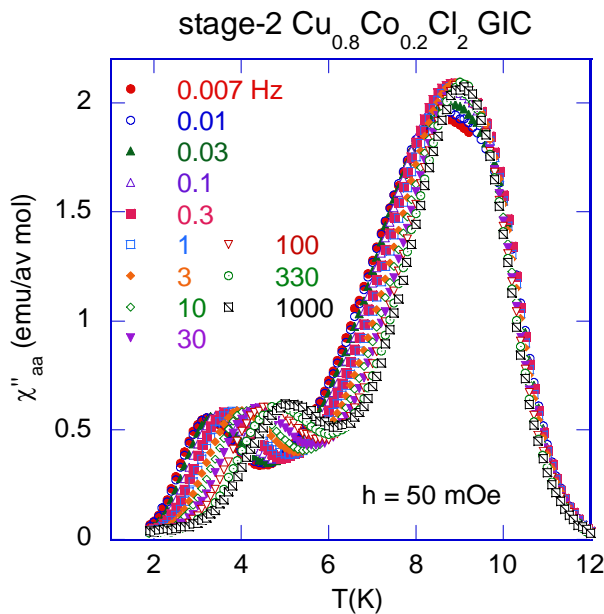

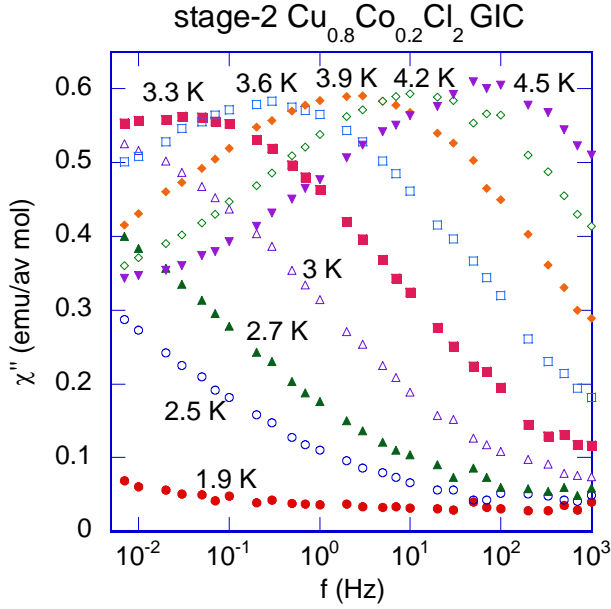Figure 6. $\chi_{aa}^{"}$ vs T for various frequencies. $c = 0.8$. $H = 0$. $h = 50$ mOe. $h \perp c$. (Suzuki, I.S., 1999b)

16

stage-2 $Cu_{0.8}Co_{0.2}Cl_2$ GIC

Figure 7. $\chi_{aa}^{''}$ vs f for various temperatures. $c = 0.8$. (Suzuki, I.S., 1999b

stage-2 $Cu_{0.8}Co_{0.2}Cl_2$ GIC
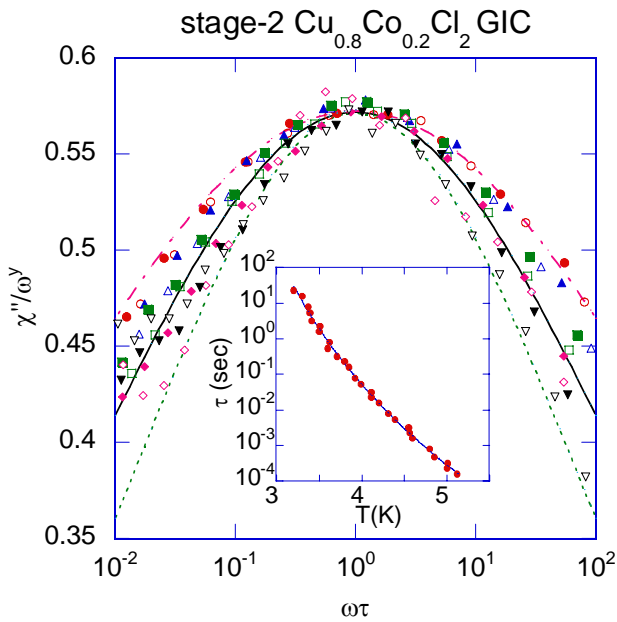
Figure 8. Plot of $\chi_{aa}^{''}/\omega^y$ as a function of $\omega\tau$ for stage-2 $Cu_cCo_{1-c}Cl_2$ GIC with $c = 0.8$, where $y = 0.0089$ and $\tau = \tau_0 (T/T^* - 1)^{-x}$ with $\tau_0 = 0.59$ sec, $x = 13.81$, and $T^* = 1.825$ K: $f = 0.01$ (●), 0.05 (○), 0.1 (▲), 0.5 (△), 1 (■), 5 (□), 10 (◆), 50 (◇), 100 (▼), and 500 Hz (▽). The plot of τ vs T is shown in the inset. The scaling function given by eqn (5) is shown by dotted line ($p = 0.7$), solid line ($p = 0.75$), and dash dotted line ($p = 0.80$), where a multiplicity constant is chosen so that the value of scaling function at $\omega\tau = 1$ coincides with the value of data. (Suzuki, I.S., 1999b)

Figure 7 shows the frequency dependence of $\chi_{aa}^{''}$ for $c = 0.8$ at various temperatures in the frequency range $0.007 \leq f \leq 1000$ Hz (Suzuki, I.S., 1999b). The absorption $\chi_{aa}^{''}$ decreases with increasing frequency below 3.3 K. It has a local maximum, shifting to the higher frequency side with increasing temperature (0.07 Hz at 3.4 K and 330 Hz at 4.9 K), and a local minimum (0.03 Hz at 4.8 K and 360 Hz at 6.4 K). This shift of local maximum indicates that the lowest

17

temperature phase is a RSG phase. The broad spectral width of up to 5.7 decades in frequency FWHM (full width at half maximum) (compared to a single time Debye fixed width of 1.14 decades) reflects an extremely broad distribution of relaxation times.

The maximum of χ''_{aa} vs f provides a method for determining an average relaxation time τ for each temperature: $\omega\tau = 1$. The inset of Fig.8 shows the average relaxation time τ as a function of temperature (Suzuki, I.S., 1998b, 1999b, Suzuki, M., 2000). It divergingly increases with decreasing temperature. The most likely source for such a dramatic divergence of τ is a critical slowing down. We assume that $\chi''_{aa}(\omega,T)$ is described by a scaling relation

$$\chi''_{aa} = A\omega^y G(\omega\tau),$$
(4)

where A is a constant, y is an exponent, and $G(\omega\tau)$ is a scaling function of $\omega\tau$ having a peak at $\omega\tau = 1$. The relaxation time τ can be described by eqn (2), where $x = z\nu$, z is the dynamic critical exponent, ν is the exponent of the spin correlation length, and T^* is a finite critical temperature. The least squares fit of the data of τ vs temperature over the temperature range of 3.2 - 5.1 K yields the parameters $x = 13.8\pm1.4$, $T^* = 1.83\pm0.21$ K, and $\tau_0 = 0.587\pm1.89$ sec. It is predicted from eqn (1) that χ''_{aa} can be described by a power-law ($\chi''_{aa} \approx \omega^y$) for $\omega\tau = 1$. The least squares fit of the data (peak value of χ''_{aa} vs f) yields the exponent $y = 0.0089 \pm 0.0003$. In Fig.8 we show the scaling plot of χ''_{aa}/ω^y as a function of $\omega\tau$. We find that almost all the data fall on a scaling function defined by

$$\frac{\chi''_{aa}}{\chi''_{aa}{}^{max}} = \frac{G(\omega\tau_h)}{G(\omega\tau_h = 1)}$$
(5)

with

$$G(\omega\tau_h) = \mathrm{Im}\left[\frac{1}{1+(i\omega\tau_h)^{1-p}}\right] = \frac{\cos(\pi p/2)/2}{\cosh[(1-p)\ln(\omega\tau_h)]+\sin(\pi p/2)}, \quad (6)$$

and $p = 0.75 \pm 0.05$ for $0.01 \le \omega\tau \le 100$, where A in eqn (4) is chosen as $A=1.146\cos(\pi p/2)/[1+\sin(\pi p/2)]$ so that $\chi_{aa}''/\omega y$ takes 0.573 at $\omega\tau = 1$. The value of $p = 0$ corresponds to the Debye equation for relaxation with a single time constant. The high value of p indicates that an extremely broad distribution of relaxation times persists throughout the whole temperature range studied.

The peak of χ_{aa}'' around 3 - 4 K for $c = 0.5$, 0.7, and 0.88 also shifts to the low temperature side with decreasing frequency. This peak is also assumed to appear when the condition $\omega\tau = 1$ is satisfied. The temperature dependence of τ is well fitted to eqn (2) for the critical slowing down, in spite of the limited data, where $T^* = 1.78 \pm 0.79$ K and $x = 12.70 \pm 5.80$ for $c = 0.5$, $T^* = 1.28 \pm 0.12$ K and $x = 12.44 \pm 0.73$ for $c = 0.7$, and $T^* = 1.90 \pm 0.19$ K and $x = 8.51 \pm 1.20$ for $c = 0.88$. Monte Carlo simulation on a short range 3D Ising SG system has predicted $x = 7.9 \pm 1.0$ (Ogielski, A.T., 1985). The value of x for $c = 0.88$ is close to this predicted value. The value of T^* is weakly dependent on Cu concentration: T^* is between 1.78 K and 1.90 K except for $c = 0.7$. These results suggest that the reentrant spin glass transition belongs to the universality class of the short range 3D Ising SG. The RSG phase may be related to a chiral SG characterized by the existence of frozen-in vortices.

3.3   Spin glass phase at c = 0.93

Figure 9 shows the temperature dependence of χ_{aa}'' for $c = 0.93$. A singe peak at T_{SG} shifts to the higher temperature side with increasing frequency. Figure 10 shows the frequency dependence of χ_{aa}'' for $c = 0.93$. This frequency dependence is rather different from that for $c = 0.8$. The absorption χ_{aa}'' decreases with increasing frequency below 5.9 K. Above 6.3 K it shows a peak, shifting to the higher frequency side with increasing

temperature. The peak of $\chi_{aa}^{"}$, T_{SG}, shifts to the low temperature side with increasing magnetic field along the c plane. The least squares fit of the data of T_{SG} vs H to the form given by eqn (3) yields the exponent $a = 3.56 \pm 0.38$. This exponent a is much larger than that (= 1.5) predicted by Almeida-Thouless (Almeida, J.R.L., 1978) for the field dependence of freezing temperature at the transition between the paramagnetic phase and the SG phase. Note that $a = 1.26 \pm 0.02$ for $c = 0.8$. The dramatic increase of τ with decreasing temperature around T_{SG} cannot be explained by a conventional critical
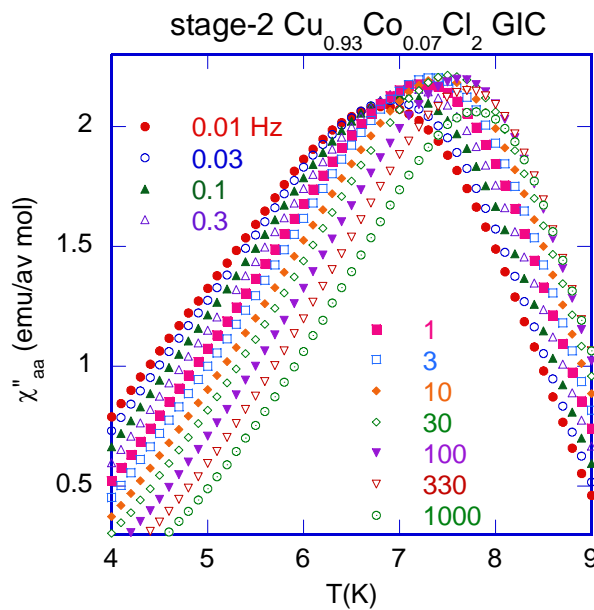

Figure 9. $\chi_{aa}^{"}$ vs T for various frequencies. $c = 0.93$. (Suzuki, M., 2000)

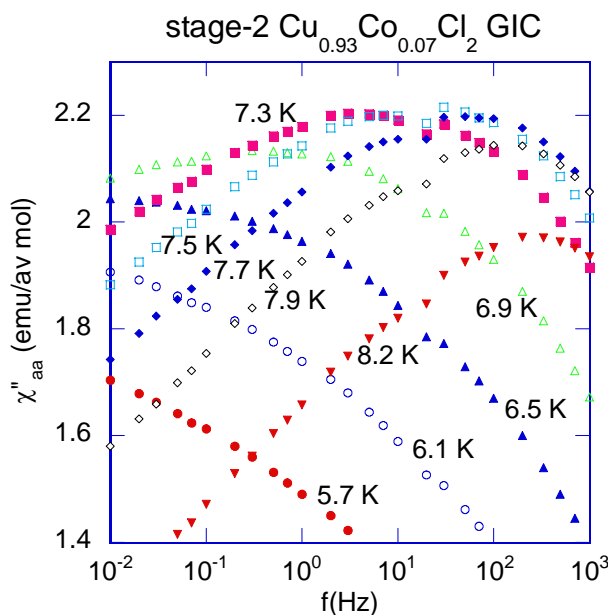Figure 10. $\chi_{aa}^{"}$ vs f for various temperatures. $c = 0.93$. (Suzuki, M., 2000)

20

slowing down. These results suggests that the nature of SG phase below T_{SG} is essentially different from that of RSG phase below T_{RSG}.

3.4   Chiral spin glass phase

It is known that XY (n = 2) spin glasses posses a twofold Ising-like degeneracy, called "chirality," in addition to a continuous degeneracy associated with the original spin-rotation symmetries (Kawamura, H., 1985, 1986, 1987, 1991, 1995). The appearance of such twofold (Z_2) chiral degeneracy is a consequence of the noncollinear or noncoplanar spin structures induced by spin frustration. Chirality physically represents the sense or the handedness of these noncollinear (or noncopolanar) spin structures. In its ordered symmetry-broken state, such noncollinear (noncoplanar) spin ordering break the full symmetry of the Hamiltonian, $O(n=2) = Z_2 \times SO(n)$.

Numerical study of the chiral ordering in vector spin glasses has been initiated for the case of the 2D XY spin glass, the simplest spin-glass model which can sustain a nontrivial chiral degree of freedom. Kawamura and Tanemura (Kawamura, 1985, 1986) have shown that the ordering tendency of the chirality seems to be much enhanced as compared with that of the XY spin. Although both the spin and chirality order only at 0 K, the chiral-glass susceptibility behaves like the spin-glass susceptibility of a pure Ising spin glass. For 3D XY spin glasses the chiral spin glass order occurs at a finite temperature without the conventional spin glass order. The chiral-glass transition belongs to the universality class of the 3D Ising spin glass.

Through a Monte Carlo study on the spin ordering process of the $2D \pm J$ plane rotator (XY) model on the square lattice, Kawamura and Tanemura have obtained the following magnetic phase diagram, where c is the concentration of AF bonds and 1-c is the concentration of F bonds. For $c \approx 0$ the system undergoes a Kosterlitz-Thouless (KT)-like transition at $T \approx J$. For $c = 0.5$ the system shows a novel type of SG transition into a chiral SG at $T \approx 0.3$ J, which is characterized with the existence of frozen-in vortices. The

nature of chiral SG is not sensitive to the concentration c. For $c < c_0$ (<0.25) the reentrance phenomena are observed with the high temperature KT phase and the low temperature chiral SG phase. In a strict sense this discussion seems to be inconsistent with the prediction that the chiral SG does not occurs at any finite temperature for the 2D XY spin glass. In spite of that, it may be reasonable to assume that the same magnetic phase diagram still holds valid for a quasi 2D XY spin glass system such stage-2 $Cu_cCo_{1-c}Cl_2$ GICs having very weak interplanar exchange interaction: the chiral SG phase appears at a finite temperature.

The Cu concentration in the system does not coincide with the concentration of antiferromagnetic bonds in the theory, because $J(Cu\text{-}Co)$ is ferromagnetic. The lattice form of the system is different from that used in the theory. The effect of interplanar interaction on the phase transition is not also taken into account in the theory. In spite of such differences, the magnetic phase diagram is qualitatively in good agreement with the prediction from the theory: (i) T_{RSG} is almost independent of Cu concentration, and (ii) the magnetic phase diagram consists of the ferromagnetic phase for $c \leq 0.3$, the high temperature ferromagnetic phase and low temperature RSG phase for $0.4 \leq c \leq 0.9$, and a SG phase for $0.9 < c \leq 0.93$.

4 $Cu_cCo_{1-c}Cl_2\text{-}FeCl_3$ GBICs ($0 \leq c \leq 1$)

4.1   *Overview*

$Cu_cCo_{1-c}Cl_2\text{-}FeCl_3$ GBICs have a c-axis stacking sequence of -G-I_1-G-I_2-G-I_1-G-I_2-G- (G = graphite layer, I_1 = $Cu_cCo_{1-c}Cl_2$ layer, and I_2 = $FeCl_3$ layer). In these compounds the $Cu_cCo_{1-c}Cl_2$ layer is formed of two different magnetic ions which are randomly distributed on the triangular lattice. The character of the average intraplanar exchange interaction in $Cu_cCo_{1-c}Cl_2$ layers changes from ferromagnetic to antiferromagnetic with increasing the Cu concentration c, while the intraplanar exchange interaction in $FeCl_3$ layers is antiferromagnetic. The magnetic properties of $Cu_cCo_{1-c}Cl_2$-

FeCl$_3$ GBICs are not simply a superposition of those of stage-2 Cu$_c$Co$_{1-c}$Cl$_2$ GIC and stage-2 FeCl$_3$ GIC. The long range spin order in the Cu$_c$Co$_{1-c}$Cl$_2$ layers is coupled with that in the FeCl$_3$ layers through an interplanar exchange interaction, leading to the helical spin order.

Suzuki et al. (Suzuki, M., 1999b, Suzuki, I.S., 1997, 2000) have studied the magnetic phase transition of these compounds using SQUID DC magnetization and SQUID AC magnetic susceptibility. They have shown that these compounds undergo magnetic phase transitions at T_h, T_{cu}, T_{cl}, T_{SG}, and T_{RSG} ($T_h > T_{cl} > T_{RSG} \approx T_{SG}$) depending on the Cu concentration. The phase transition at T_h is related to a helical spin order. The phase transitions at T_{cu} and T_{cl} are associated with a spin order of Cu$_c$Co$_{1-c}$Cl$_2$ layers. The reentrant spin glass (RSG) phase below T_{RSG} for $c \leq 0.4$ and the spin glass (SG) phase below T_{SG} for $c \geq 0.5$ are due to the spin frustration effect occurring in FeCl$_3$ layers.

4.2 SQUID AC magnetic susceptibility

Figures 11(a) and (b) show the temperature dependence of χ''_{aa} of GBIC with $c = 0$,
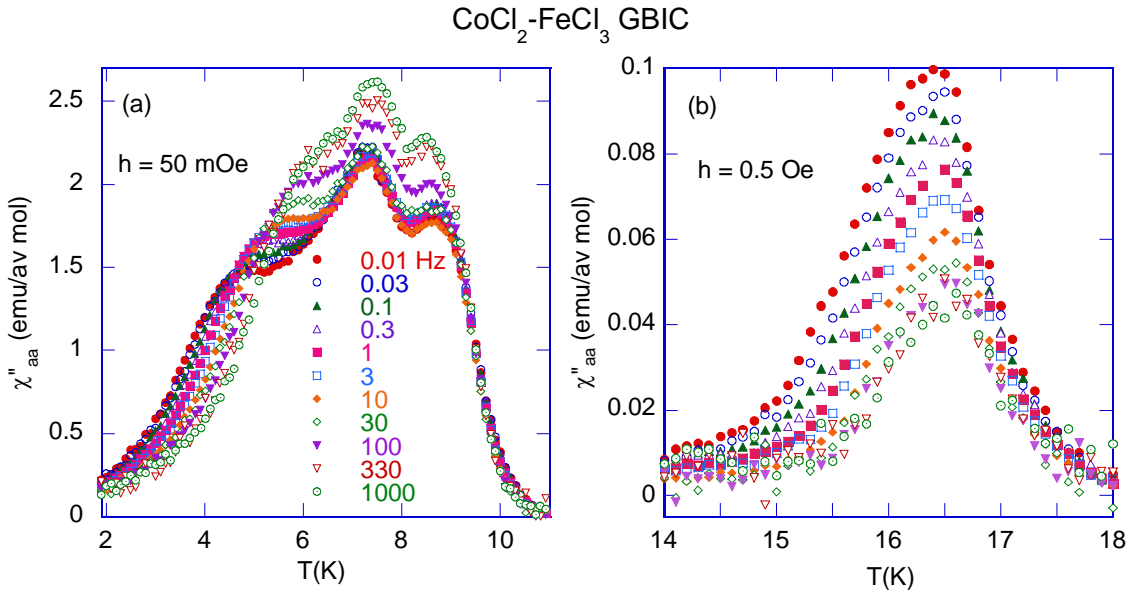

Figure 11. Temperature dependence of χ''_{aa} for GBIC with $c = 0$ at various frequencies. $H = 0$ and $h \perp c$. (a) $1.9 \leq T \leq 11$ K. $h = 50$ mOe. (b) $14 \leq T \leq 18$ K. $h = 0.5$ Oe. (Suzuki, M., 1999b)

23

where h = 50 mOe for (a) and h = 0.5 Oe for (b) (Suzuki, M., 1999b). This compound undergoes four magnetic phase transitions at T_h (= 16.3 K), T_{cu} (= 8.5 - 8.6 K), T_{cl} (= 7.3 - 7.4 K), and T_{SG} (= 4.7 - 5.9 K). The absorption χ_{aa}'' has a shoulder at T_{SG} which increases with increasing frequency (5 K at f = 0.01 Hz and 5.8 K at f = 1 kHz). Note that the frequency dependence of T_{SG} is almost the same as that of $T_{SG}^{(h)}$ for stage-2 $FeCl_3$ GIC (Suzuki, M., 1998c). *The* peak at T_{SG} shifts to the low temperature side with increasing magnetic field along the c plane. The peak temperature is related to the field H through a power law form given by eqn (3), where $T_{SG}(H=0)$ = 5.90 K, H_0 = 0.34 kOe, a = 1.224 ± 0.116 (H = 0 - 70 Oe) for $CoCl_2$-$FeCl_3$ GBIC and $T_{SG}^{(h)}(H=0)$ = 5.69 K, H_0 = 2.15 kOe, a = 1.423 ± 0.142 (H = 0 - 500 Oe) for stage-2 $FeCl_3$ GIC. The value of a obtained is a little smaller than that (a = 1.50) predicted by Almeida and Thouless (Almeida, J.R.L., 1978).

The absorption χ_{aa}'' of GBIC with c = 0 has also two peaks at T_{cl} and T_{cu}. The value of T_{cl} slightly increases with increasing frequency (7.3 K at f = 0.01 Hz and 7.4 K at f = 1 kHz), while the value of T_{cu} seems to decrease slightly with increasing frequency (8.6 K at f = 0.01 Hz and 8.5 K at f = 1 kHz. In stage-2 $CoCl_2$ GIC χ_{aa}'' has two peaks at T_{cl} (Co) and T_{cu} (Co) (Suzuki, M., 1998a). The value of T_{cl} (Co) slightly increases with increasing frequency (6.9 K at f = 0.1 Hz to 7.1 K at f = 1 kHz), while the value of T_{cu} (Co) (= 8.9 K) is independent of frequency. Note that the value of T_{cl} is a little higher than that of T_{cl}(Co) and that the value of T_{cu} is a little lower than T_{cu}(Co).

The absorption χ_{aa}'' of GBIC with c = 0 has a peak at T_h, which coincides with the peak temperature of χ_{aa}'. The peak slightly shifts to the high temperature side with increasing frequency (16.4 K at f = 0.01 Hz and 16.6 K at f = 1 kHz), while the peak height dramatically decreases with increasing frequency. This peak shifts to the low temperature side with increasing magnetic field (15.8 K at H = 1 Oe) along the c plane, while the peak height dramatically decreases with increasing field and completely disappears above 2 - 3 Oe. The peak temperature T_h is related to the field H through a

power law similar to eqn (3), where $a = 1.4 \pm 0.2$, $T_h(H=0) = 16.4$ K, and $H_0 = 79 \pm 5$ Oe. This result suggests that the resultant interplanar interaction has an antiferromagnetic character.

Figures 12(a) and (b) show the temperature dependence of χ''_{aa} for GBIC with $c = 0.2$ (Suzuki, I.S., 1997, 2000). The absorption χ''_{aa} shows a small peak at T_h (=16.2 K), a
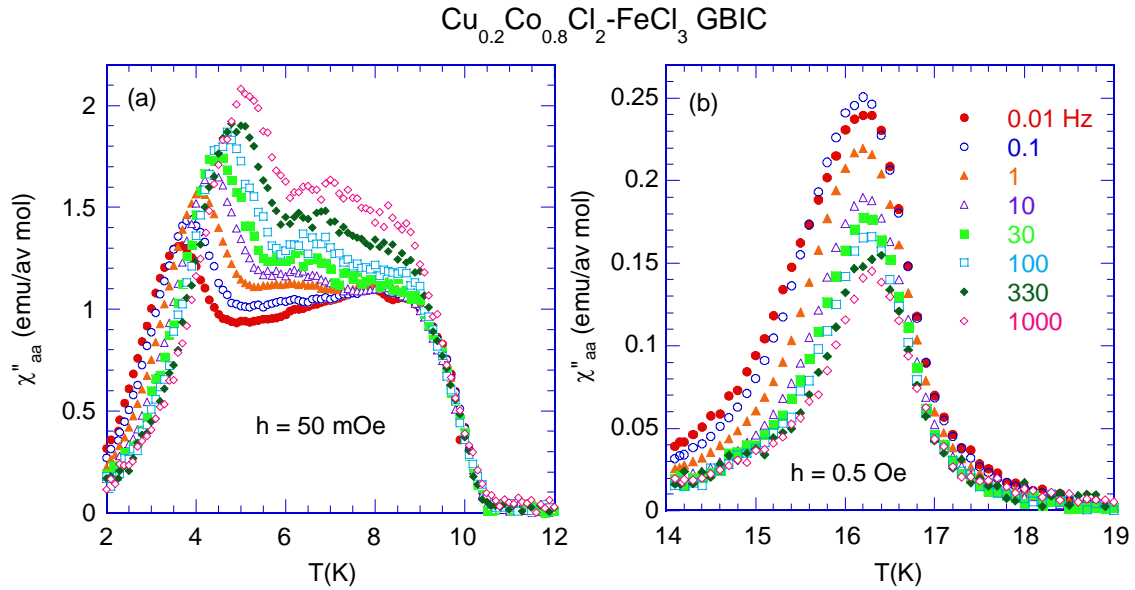

Figure 12. χ''_{aa} vs T for GBIC with $c = 0.2$ at various frequencies. $H = 0$. $h \perp c$. (a) $1.9 \leq T \leq 10$ K and $h = 50$ mOe. (b) $14 \leq T \leq 19$ K and $h = 0.5$ Oe. (Suzuki, I.S., 2000)
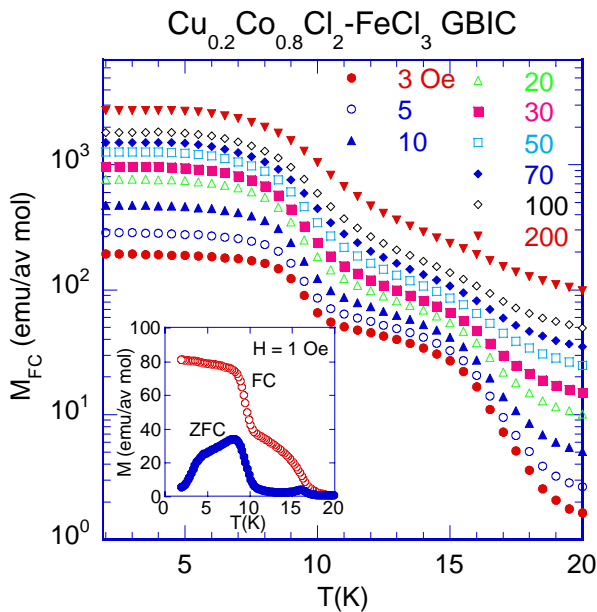

Figure 13. (a)Field dependence of M_{FC} for GBIC with $c = 0.2$ at various temperatures. $H \perp c$. The temperature dependence of M_{FC} and M_{ZFC} for $c = 0.2$ is shown in the inset. $H = 1$ Oe. (Suzuki, I.S., 2000)

very broad peak at T_{cu} ($\approx$ 7.9 K), a small peak at T_{cl} ($\approx$ 6.2 - 6.4 K), and a sharp peak at

T_{RSG}. The peak at T_{RSG} shifts to the high temperature side with increasing frequency.

The peak temperature T_h shifts to the low temperature side with increasing field along the

c plane, while the peak height drastically decreases and disappears above 7 Oe. This

result suggests that the resultant interplanar exchange interaction is antiferromagnetic and

weak.

Figure 13 shows the temperature dependence of M_{FC} for c = 0.2 in the presence of H

($\geq$2 Oe) along the c plane (Suzuki, I.S., 2000). The increase of M_{FC} with decreasing

temperature is made in two steps: it starts to increase at T_h and drastically increases

below 10 K, and reaches a saturated value below T_{cl}. The inset of Fig.13 shows the

temperature dependence of M_{ZFC} and M_{FC} for c = 0.2, where H (= 1 Oe) is applied along

the c plane. M_{ZFC} has a small peak at T_h = 16.0 K, a large peak at T_{cu} = 8.1 K, and a

shoulder around T_{RSG} = 3.7 - 4.5 K. The deviation of M_{ZFC} from M_{FC} occurs below 21.3

K, indicating a irreversible effect of magnetization.

Figures 14(a) and (b) show the temperature dependence of $\chi_{aa}^{''}$ for GBICs with c =

0.4 and c = 0.5, respectively (Suzuki, I.S., 2000). For c = 0.4 $\chi_{aa}^{''}$ has a very broad peak at
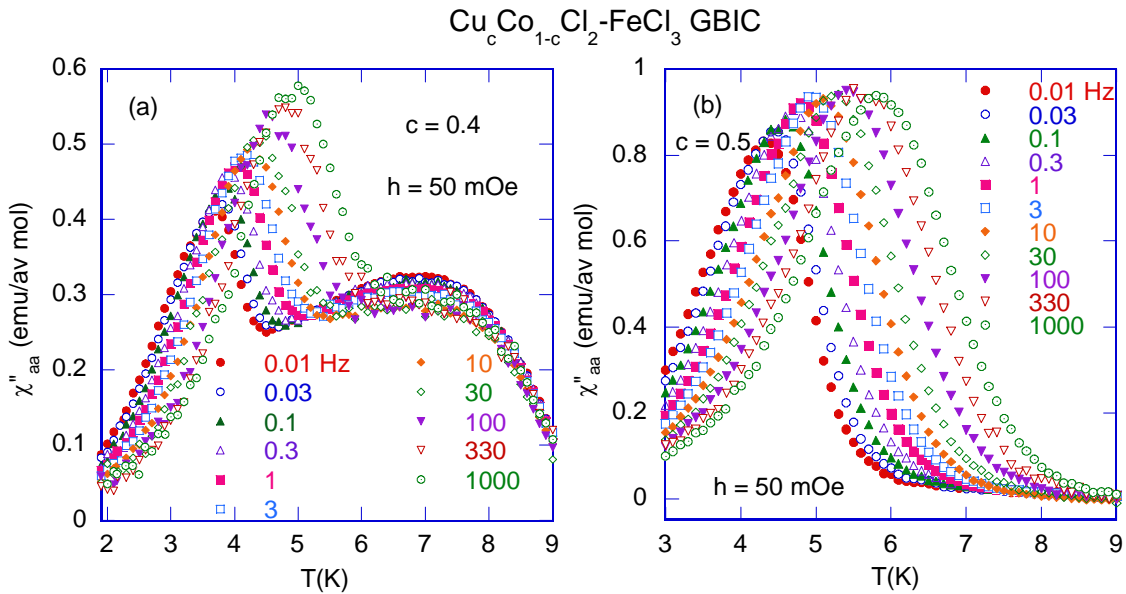

Figure 14. $\chi_{aa}^{''}$ vs T for (a) c = 0.4 and (b) c = 0.5 at various frequencies. H = 0. $h \perp c$.
(Suzuki, I.S., 2000)

T_{cu} (= 6.9 K) and a sharp peak at T_{RSG}. The peak at T_{RSG} shifts to the high temperature side with increasing frequency. No anomaly in χ''_{aa} is observed around 16 K. For $c = 0.5$ χ''_{aa} has a single peak at a temperature defined as T_{SG}, shifting to the high temperature side with increasing frequency.

4.3   Magnetic phase diagram

Figure 15 shows the magnetic phase diagram for GBICs. The critical temperatures T_h, T_{cu}, T_{cl}, and T_{RSG}, and T_{SG} are defined as temperatures at which χ''_{aa} at $f = 0.1$ Hz has peaks. The result is summarized as follows: (i) T_h (≈ 16 K) and T_{cl} are observed only for $0 \leq c \leq 0.2$, (ii) T_{cu} and T_{cl} decrease with increasing Cu concentration and tend to reduce to zero around $c = 0.5$, (iii) T_{RSG} for $c \leq 0.4$ and T_{SG} for $c \geq 0.5$ are almost independent of Cu concentration. A helical spin order occurs below T_h. Below T_{cu} two-dimensional (2D) ferromagnetic long range order appears in each $Cu_cCo_{1-c}Cl_2$ layer. Below T_{cl} these 2D ferromagnetic $Cu_cCo_{1-c}Cl_2$ layers are antiferromagnetically stacked along the c axis, forming a 3D antiferromagnetic phase. The spin glass phase occurs below T_{RSG} or T_{SG} in each $FeCl_3$ layer.

In the inset of Fig.15 we show the frequency dependence of T_{RSG} for GBICs with $c =$

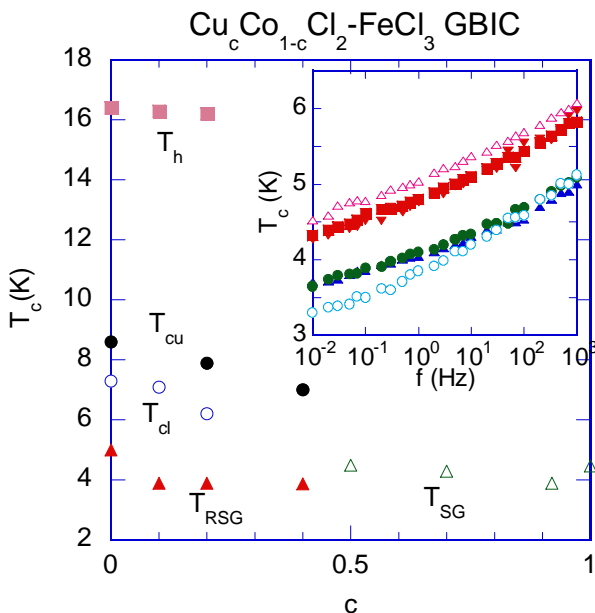Figure 15. Magnetic phase diagram of GBICs. T_h, T_{cu}, T_{cl}, T_{RSG}, and T_{SG} correspond to the peak temperatures in χ''_{aa} vs T at $f = 0.1$ Hz. The inset shows the frequency dependence of T_{SG} and T_{RSG} for GBICs with $c = 0.2$ (●), 0.4 (▲), 0.5 (■), and 1 (▼), stage-2 $Cu_cCo_{1-c}Cl_2$ GIC with $c = 0.8$ (○), and stage-2 $FeCl_3$ GIC (Δ). (Suzuki, I.S., 2000)

0.2 and 0.4, T_{SG} for GBICs with $c = 0.5$ and 1, T_{RSG} for stage-2 $Cu_cCo_{1-c}Cl_2$ GIC with c

$= 0.8$ and T_{SG} for stage-2 $FeCl_3$ GIC. The frequency dependence of T_{SG} for GBICs with

$c = 0.5$ and 1 is almost the same as that of T_{SG} for stage-2 $FeCl_3$ GIC. This result

suggests that for GBICs for $0.5 \leq c \leq 1$ the SG behavior occurs in the $FeCl_3$ layer. Note that

the value of T_{RSG} for GBICs with $c = 0.2$ and 0.4 is lower than that of stage-2 $FeCl_3$ GIC

at the same frequency, but is rather close to that of T_{RSG} for stage-2 $Cu_cCo_{1-c}Cl_2$ GIC

with $c = 0.8$. In GBICs with $c = 0.2$ and 0.4 the RSG behavior occurring inside the $FeCl_3$

layers may be modified by the random field effect arising from adjacent $Cu_cCo_{1-c}Cl_2$

layers. Because of the ferromagnetic spin order in $Cu_cCo_{1-c}Cl_2$ layers, the uniform

interplanar exchange field may generate a random staggered magnetic field in each Fe^{3+}

(Fe^{2+}) spin of the $FeCl_3$ layers. The absorption $\chi_{aa}^{''}$ for GBICs with $c = 0.2$ and 0.4

shows a plateau-like form between T_{cu} and T_{cl}, indicating that the phase transitions at T_{cu}

and T_{cl} are partially destroyed by random field effects arising from the adjacent $FeCl_3$

layers through competing interplanar exchange interactions.

4.4   Helical spin order at T_h

The phase transition at T_h is observed only in the system ($0 \leq c \leq 0.2$) where T_{cu} or T_{cl}

are also observed. This result indicates that the helical spin order at T_h arises from

competing interplanar exchange interactions. Because of weak interactions the phase

transition at T_h is destroyed by a very weak magnetic field H_t (≈ 3 Oe for $c = 0.2$) along

the c plane. In spite of the complicated intraplanar and interplanar exchange interactions,

for simplicity we consider the model of $CoCl_2$-$FeCl_3$ GBIC which is regarded as a 1D

spin system: Co^{2+} and Fe^{3+} spins are alternatively arranged at equal distances along the c

axis.

The c axis repeat distance of this system is d ($=18.77 \pm 0.46$ Å) and distance between

Co^{2+} and Fe^{3+} is $d/2$. The ground-state energy U_G of this system is described by

$$U_G = -AJ(Q_c), \tag{7}$$

where A is a positive constant, Q_c is the component of wavevector $\boldsymbol{Q}$ along the c axis, and $J(Q_c)$ is given by

$$J(Q_c) = \sum_{<i,j>} J_{ij} \exp(iQ_c R_{ij}^z). \tag{8}$$

We assume that $J'_{Co\text{-}Fe}$ is the N.N. interplanar interaction between $CoCl_2$ and $FeCl_3$ layers, $J'_{Co\text{-}Co}$ is the N.N. interplanar interactions between adjacent $CoCl_2$ layers, and $J'_{Fe\text{-}Fe}$ is the N.N. interplanar interactions between adjacent $FeCl_3$ layers. Then $J(Q_c)$ is described as

$$J(Q_c) = 2\tilde{J}'_{Co\text{-}Fe} \cos(\theta) + (\tilde{J}'_{Co\text{-}Co} + \tilde{J}'_{Fe\text{-}Fe})\cos(2\theta) + const., \tag{9}$$

where $\tilde{J}'_{Co\text{-}Fe} = J'_{Co\text{-}Fe} S_{Co}^{\perp} S_{Fe}^{\perp}$, $\tilde{J}'_{Co\text{-}Co} = J'_{Co\text{-}Co} S_{Co}^{\perp} S_{Co}^{\perp}$, and $\tilde{J}'_{Fe\text{-}Fe} = J'_{Fe\text{-}Fe} S_{Fe}^{\perp} S_{Fe}^{\perp}$, $S_{Co}^{\perp}$ and $S_{Fe}^{\perp}$ are the XY-components of spin vectors at the lattice sites of Co^{2+} and Fe^{3+} ions, respectively, and $\theta = Q_c d/2$ is the rotation angle between spins in the adjacent layers. The ground state energy becomes minimum when $J(\theta)$ has a maximum for $\theta = \theta_0$: $dJ(\theta)/d\theta = 0$ and $d^2 J(\theta)/d\theta^2 < 0$. From the condition $dJ(\theta)/d\theta = 0$ we obtain the following three cases: (i) $\theta = 0$, (ii) $\theta = \pi$, or (iii) $\cos\theta = -J_1'/2J_2'$, where J_1' and J_2' are effective interplanar exchange interactions defined as $J_1' = \tilde{J}'_{Co\text{-}Fe}$ and $J_2' = \tilde{J}'_{Co\text{-}Fe} + \tilde{J}'_{Fe\text{-}Fe}$, respectively. The case (i) corresponding to a ferromagnetic spin configuration is realized under the conditions $J_1' + 2J_2' > 0$ and $J_1' > 0$. The case (ii) corresponding to an antiferromagnetic spin configuration is realized under the conditions $-J_1' + 2J_2' > 0$ and $J_1' < 0$. The case (iii) corresponding to a helical spin configuration is realized under the conditions $J_2' < 0$ and $2|J_2'| > |J_1'|$.

In order to check which condition is satisfied, we estimate the magnitude of J'_{Co-Fe}, J'_{Co-Co}, and J'_{Co-Fe} as follows. We know that the magnetic phase transition at $T_h(GBIC)$ is destroyed by a very weak magnetic field ($H_t \approx 3$ Oe) along the c plane. This magnetic field H_t at 0 K may be described by

$$H_t \approx -\frac{<z'>(2J'_1 + J'_2)}{\mu_B[g_a(Co)S^{\perp}_{Co} + g_a(Fe)S^{\perp}_{Fe}]},$$
(10)

in terms of the above 1D chain model, where $<z'>$ is an average number of the nearest neighbor atoms. The minus sign of eqn (10) comes from the fact that the average interplanar exchange interaction is antiferromagnetic. When it is assumed that $<z'> = 6$, the interplanar interaction $(2J_1' + J_2')$ is roughly estimated as $- 0.93 \times 10^{-4}$ H_t [K]: $(2J_1' + J_2') = - 2.8 \times 10^{-4}$ K for $H_t = 3$ Oe. The value of J_2' may be roughly estimated as follows. According to Yeh et al. (Yeh, N.C., 1989) the dominant interplanar exchange interaction in stage-1 $CoCl_2$ GIC is the superexchange interaction, while both the dipole-dipole interaction and superexchange interaction are equally important in stage-2 $CoCl_2$ GIC. For higher stage $CoCl_2$ GICs, the dipole-dipole interaction dominates because of the rapid decrease of the superexchange interaction with increasing stage number. Because of the large separation distance the interplanar exchange interaction J'_{Co-Co} and J'_{Fe-Fe} in $CoCl_2$-$FeCl_3$ GBIC may be described by the dipole-dipole interaction between S_i and S_m,

$$H_{d-d} = (g_a\mu_B)^2\left[\frac{\mathbf{S}_i \cdot \mathbf{S}_m}{R_{im}^3} - \frac{3(\mathbf{S}_i \cdot \mathbf{R}_{im})(\mathbf{S}_m \cdot \mathbf{R}_{im})}{R_{im}^5}\right].$$
(11)

Since the direction of spin $\mathbf{S}_i$ is perpendicular to $\mathbf{R}_{im}$, the Hamiltonian H_{d-d} can be approximated as a form of $-2J_{d-d}(\mathbf{S}_i\mathbf{S}_m)$ where $J_{d-d} = (g_a\mu_B)^2/2(R_{im})^3$ is positive and favors the antiferromagnetic interplanar exchange interaction. Then the values of J'_{Co-Co}

30

and J'_{Fe-Fe} can be estimated as $J'_{Co-Co} = -1.9 \times 10^{-3}$ and $J'_{Fe-Fe} = -1.9 \times 10^{-4}$ K, respectively, where $g_a(Co) = 6.40$, $g_a(Fe) = 2.03$, and $R_{im} \approx 18.77$ Å. Then we have $J_1' = 7.0 \times 10^{-4}$ K and $J_2' = -1.66 \times 10^{-3}$ K using the relation $2J_1' + J_2' = -2.8 \times 10^{-4}$ K. This rough estimate may satisfy the condition for the occurrence of helical spin structure: $J_2' < 0$ and $|2J_2'|/|J_1'| > 1$. Using these values of J_1' and J_2' the rotation angle θ is calculated as 78°, which is close to an angle (72°) of helical spin structure with periodicity $5d$ (= 10 magnetic layers). This period is smaller than ξ_c ($\approx$ 20 magnetic layers) in stage-1 $CoCl_2$ GIC (Ikeda, H., 1985).

4.5   Random field effect near T_{cu} and T_{cl}

Next we consider a possibility that the spin glass phase transition of $FeCl_3$ layers at T_{SG} is affected by random field effects in $CoCl_2$-$FeCl_3$ GBIC. We assume that the $FeCl_3$ layers in $CoCl_2$-$FeCl_3$ GBIC can also be regarded as 2D XY random spin systems with a mixture of Fe^{3+} and Fe^{2+} spins. Because of the ferromagnetic spin order in $CoCl_2$ layers, the interplanar exchange field is uniform and equivalent for each Fe^{3+} (Fe^{2+}) spin. Thus the $FeCl_3$ layers of $CoCl_2$-$FeCl_3$ GBIC magnetically behave like an XY-like antiferromagnetic random spin system in the presence of a uniform interplanar exchange field along the c plane. This uniform magnetic field is expected to generate a random staggered magnetic field, giving rise to the random field effect (Fishman, S., 1979) The absorption χ_{aa}'' of stage-2 $FeCl_3$ GIC has a sharp peak at $T_{SG}^{(h)}(Fe)$ (see Fig.7.32(a)), while χ_{aa}'' of $CoCl_2$-$FeCl_3$ GBIC has a shoulder around T_{SG}. These results clearly indicate that the spin glass phase below T_{SG} is partially destroyed by the random field along the c plane.

Since short range spin order with antiferromagnetic character develops in the $FeCl_3$ layers at temperatures well above T_{SG}, the interplanar exchange field H'_E may have a random field character whose magnitude and direction are different depending on the Co^{2+} lattice sites [$<H'_E> = 0$ and $<(H'_E)^2> \neq 0$)]. It is predicted from a random field

theory that the ferromagnetic long range spin order of Co^{2+} is destroyed by this random field since the dimension of this system is 2D (Imry, Y., 1975). The dispersion χ'_{aa} of stage-2 $CoCl_2$ GIC has a rather sharp peak at the peak temperature T_p between T_{cu} and T_{cl}, while χ'_{aa} of $CoCl_2$-$FeCl_3$ GBIC has a very broad peak. Such a plateau-like form between T_{cu} and T_{cl} indicates that a 2D long range spin order in $CoCl_2$ layers is partially destroyed by a random field arising from the adjacent $FeCl_3$ layers.

REFERENCES

Birgeneau, R.J., R.A. Cowley, G. Shirane, and H. Yoshizawa, J. Statistical Phys. 34: 817, 1984. See also references therein for experimental works.

Chehab, S., P. Biensan, J. Amiell, and S. Flandrois. *J. de Physique* I 1: 537, 1991.

Chehab, S., P. Biensan, S. Flandrois, and J. Amiell. *Phys. Rev. B* 45: 2844-54, 1992.

de Almeida, J.R.L. and D.J. Thouless. *J. Phys. A* 11: 983, 1978.

Essam, J.W. *Phase transitions and critical phenomena* (ed. C. Domb, M.S. Green) Vol.2, p.197, Academic Press, London, 1972.

Fishman S. and A. Aharony. *J. Phys. C* 12: L729, 1979.

Flandrois, S., P. Biensan, J.M. Louis, G. Chouteau, T. Roisnel, G. Andre, and F. Bouree. *Mol. Cryst. Liq. Cryst*. 245: 105, 1994.

Hérold, A., G. Furdin, D. Guerard, L. Hachgim, M. Lelaurain, N.E. Nadi, and R. Vangelisti. *Synth. Met*.:12, 11, 1985.

Ikeda, H., Y. Endoh, and S. Mitsuda. *J. Phys. Soc. Jpn*. 54: 3232, 1985.

Imry, Y. and S.K. Ma. *Phys. Rev. Lett*. 35: 1399, 1975.

Kawamura, H. and M. Tanemura. *J. Phys. Soc. Jpn*. 54: 4479, 1985.

Kawamura, H. and M. Tanemura. *J. Phys. Soc. Jpn*. 55: 1802, 1986.

Kawamura, H. and M. Tanemura. *Phys. Rev. B* 36: 7177, 1987.

Kawamura, H. and M. Tanemura. *J. Phys. Soc. Jpn*. 60: 608, 1991.

Kawamura, H. *Phys. Rev. B* 51: 12398, 1995

Mydosh, J.A. *Spin glasses: an experimental introduction*, Taylor and Francis, London, 1993.

Nicholls, J.T. and G. Dresselhaus. *Phys. Rev. B* 41: 9744, 1990b.

Niess, R. and E. Stumpp. *Carbon* 16: 265, 1978.

Ogielski, A. T. Phys. *Rev. B* 32: 7384, 1985.

Rancourt, D.G., B. Hun, and S. Flandrois. *Can. J. Phys*. 66: 776, 1988.

Rancourt, D.G., S. Flandrois, P. Biensan, and G. Lamarche. *Can. J. Phys*. 68: 1435, 1990.

Rosenman, I., F. Batallan, Ch. Simon, and L. Hachim, *J. de Physique* 47: 1221, 1986.

Stinchcombe, R.B. *Phase Transitions and Critical Phenomena* (ed. C. Domb, J.L. Lebowitz) vol. 7, p.151, Academic Press, London, 1983. See also references therein for theoretical works.

Suzuki, I.S., M. Suzuki, L.F. Tien, and C.R. Burr. *Phys. Rev. B* 43: 6393, 1991.

Suzuki, I.S., F. Khemai, M. Suzuki, and C.R. Burr. *Phys. Rev. B* 45: 4721, 1992.

Suzuki, I.S., C. J. Hsieh, F. Khemai, C.R. Burr, and M. Suzuki. *Phys. Rev. B* 47: 845, 1993b.

Suzuki, I.S., C. Vartuli, C.R. Burr, and M. Suzuki. *Phys. Rev. B* 50: 12568, 1994a.

Suzuki, I.S., C.J. Hsieh, F. Khemai, C.R. Burr, M. Suzuki, and Y. Maruyama. *Mol. Cryst. and Liq. Cryst.* 245: 99-104, 1994b.

Suzuki, I.S. and M. Suzuki. *Phys. Rev. B* 51: 8230, 1995.

Suzuki, I.S., M. Suzuki, H. Sato, and T. Enoki. *Solid State Commun.* 104: 581, 1997.

Suzuki, I.S. and M. Suzuki. *Solid State Commun.* 106: 513, 1998b.

Suzuki, I.S. and M. Suzuki. *Phys. Rev. B* 59: 6943, 1999a.

Suzuki, I.S. and M. Suzuki. *J. Phys. Condensed Matter* 11: 521,1999b.

Suzuki, I.S., M. Suzuki, H. Satoh, and T. Enoki. *Mol. Cryst. Liq. Cryst.* 34:107, 2000.

Suzuki, M., I. Oguro, and Y. Jinzaki. *J. Phys. C* 17: L575, 1984b.

Suzuki, M., I.S. Suzuki, W. Zhang, F. Khemai, and C.R. Burr. *Phys. Rev. B* 46: 5311, 1992.

Suzuki, M., I.S. Suzuki, M. Johnson, J. Morillo, and C.R. Burr. *Phys. Rev. B* 50: 205, 1994b.

Suzuki, M. and I.S. Suzuki. *Phys. Rev. B* 58: 840, 1998a.

Suzuki, M. and I.S. Suzuki. *Phys. Rev. B* 57: 10674, 1998b.

Suzuki, M. and I.S. Suzuki. *Phys. Rev. B* 58: 371, 1998c.

Suzuki, M. and I.S. Suzuki. *Phys. Rev. B* 59: 4221, 1999b.

Suzuki, M. and I.S.. Suzuki. *Mol. Cryst. Liq. Cryst.* 34:1, 2000.

Yeh, M., I.S. Suzuki, M. Suzuki, and C.R. Burr. *J. Phys. Condensed Matter* 2: 9821, 1990.

Yeh, N.C., K. Sugihara, M.S. Dresselhaus, and G. Dresselhaus. *Phys. Rev. B* 40: 622, 1989.